Laffon et al. EJNMMI Research (2018) 8:24
https://doi.org/10.1186/s13550-018-0369-5

EJNMMI Research

ORIGINAL RESEARCH Open Access

Comparison of three-parameter kinetic model analysis to standard Patlak's analysis in ^{18}F-FDG PET imaging of lung cancer patients

E. Laffon[1,2,6*], M. L. Calcagni[4], G. Galli[4], A. Giordano[4], A. Capotosti[5], R. Marthan[1,2] and L. Indovina[3]

Abstract

Background: Patlak's graphical analysis can provide tracer net influx constant (Ki) with limitation of assuming irreversible tracer trapping, that is, release rate constant (k_b) set to zero. We compared linear Patlak's analysis to non-linear three-compartment three-parameter kinetic model analysis (3P-KMA) providing Ki, k_b, and fraction of free ^{18}F-FDG in blood and interstitial volume (V_b).

Methods: Dynamic PET data of 21 lung cancer patients were retrospectively analyzed, yielding for each patient an ^{18}F-FDG input function (IF) and a tissue time-activity curve. The former was fitted with a three-exponentially decreasing function, and the latter was fitted with an analytical formula involving the fitted IF data (11 data points, ranging 7.5–57.5 min post-injection). Bland-Altman analysis was used for Ki comparison between Patlak's analysis and 3P-KMA. Additionally, a three-compartment five-parameter KMA (5P-KMA) was implemented for comparison with Patlak's analysis and 3P-KMA.

Results: We found that 3P-KMA Ki was significantly greater than Patlak's Ki over the whole patient series, + 6.0% on average, with limits of agreement of ± 17.1% (95% confidence). Excluding 8 out of 21 patients with $k_b > 0$ deleted this difference. A strong correlation was found between Ki ratio (=3P-KMA/Patlak) and k_b ($R = 0.801$; $P < 0.001$). No significant difference in Ki was found between 3P-KMA versus 5P-KMA, and between 5P-KMA versus Patlak's analysis, with limits of agreement of ± 23.0 and ± 31.7% (95% confidence), respectively.

Conclusions: Comparison between 3P-KMA and Patlak's analysis significantly showed that the latter underestimates Ki because it arbitrarily set k_b to zero: the greater the k_b value, the greater the Ki underestimation. This underestimation was not revealed when comparing 5P-KMA and Patlak's analysis. We suggest that further studies are warranted to investigate the 3P-KMA efficiency in various tissues showing greater ^{18}F-FDG trapping reversibility than lung cancer lesions.

Keywords: ^{18}F-FDG PET, Patlak's analysis, Reversible trapping, Uptake/release rate constant, lung cancer

* Correspondence: elaffon@u-bordeaux2.fr
[1]Departments of Nuclear Medicine & Lung Function Testing, CHU de Bordeaux, Bordeaux, France
[2]Centre de Recherche Cardio-Thoracique, INSERM U-1045, Univ. Bordeaux, Bordeaux, France
Full list of author information is available at the end of the article

Background

Positron emission tomography using [^{18}F]fluorodeoxyglucose (^{18}F-FDG PET) imaging in oncology patients allows physicians to quantify the increased glycolysis of cancer cells [1]. In clinical routine, a tracer uptake index is easily available and thus widely used, namely, the standardized uptake value (SUV) [2, 3]. However, many factors can influence the SUV outcome such as the uptake time, as reported for example in lung tumors [4]. This is the reason why, besides the SUV index, different quantitative parameters that may be obtained from kinetic model analyses (KMAs) have been implemented in a number of studies investigating various tissues [5–13]. These kinetic parameters more accurately describe the tracer trapping and may be useful to better characterize different tumor types or assess treatment response [14]. The KMAs both require a dynamic acquisition over the tissue of interest to obtain its time-activity-curve (TAC) and a serial blood sampling to estimate the so-called input function (IF, i.e., ^{18}F-FDG blood TAC). Among these KMAs, Patlak's analysis is usually considered as a gold standard that provides the ^{18}F-FDG net influx constant (i.e., the uptake rate constant, Ki) from a linear fitting of graphical data [7]. However, it assumes an irreversible tracer trapping, a well-identified drawback since numerous studies have shown trapping reversibility in various tissues, either under physiological or pathological conditions [6, 9–11, 15].

Assuming that there may be a slow loss of the trapped tracer to the blood, i.e., a reversible trapping, Patlak and Blasberg derived a generalized non-linear equation including a release rate constant (k_b) in an exponential term [8]. This non-linear equation may be addressed by using an analytical approach, leading to a three-compartment three-parameter KMA (3P-KMA). 3P-KMA has been applied to healthy human lung and liver, allowing assessment of both Ki (in mL min^{-1} mL^{-1}), k_b (in min^{-1}), and fraction of free ^{18}F-FDG in blood and interstitial volume (V_b; no unit; < 1; also called total blood volume distribution) [12, 15]. It relies on an analytical solution of the non-linear Patlak's equation that requires to use an IF as a sum of exponentially decreasing functions and up to three functions may usually describe the ^{18}F-FDG IF [16, 17]. Then, it leads to a non-linear formula that is used to fit the experimental tissue TAC by simply adjusting the three above-mentioned kinetic parameters, i.e., without any tissue TAC data transform.

To the best of our knowledge, comparison between non-linear fitting by 3P-KMA and linear fitting by standard Patlak's analysis that assumes an irreversible tracer trapping has not been reported so far, whatever the tissue either under physiological or pathological conditions. Therefore, the primary aim of this study was to make this comparison in a series of lung cancer patients that was previously acquired [13]. Additionally, Ki, k_b, and V_b outcomes obtained from 3P-KMA were compared to those obtained from a three-compartment five-parameter KMA (5P-KMA) that is usually considered as a reference model when tracer trapping is reversible. Actually, 5P-KMA provides four kinetic (micro)parameters (and V_b) from which Ki and k_b may be computed, whereas the non-linear fitting of the 3P-KMA provides Ki and k_b without any additional computing.

Methods

Patients

Dynamic data of 21 patients (8 females, 13 males, 71 years old on average, range 40–86) with non-small cell lung cancer obtained from a previous prospective study were retrospectively analyzed [13]. All patients who were enrolled in the prospective study provided written informed consent before participating in it, and the further retrospective study received the approval of the ethics committees of our teaching hospitals. The patients' mean weight and height were 68 kg (range, 50–85) and 169 cm (range, 150–180), respectively. After 6 h of fasting before the tracer injection, the preinjection average plasma glucose concentration was 1.08 g L^{-1} (range, 0.87–1.28). The lesion mean size was 31.8 mm (range, 14.7–52.2).

PET imaging and data processing

PET imaging procedure has been previously described in details [13]. Briefly, a low dose CT scan was performed (75 mA, 120 kV, pitch 0.938, rotation time 0.5 s) for attenuation correction of PET emission data and for morphologic information. Then, after an intravenous bolus injection of ^{18}F-FDG (mean 237 MBq; range, 134–507) in a cannula previously inserted in the vein of the arm, a 3D thorax dynamic list-mode acquisition protocol was started lasting 60 min (Gemini GXL, Philips Medical System, Cleveland, USA; no respiratory gating). Images were reconstructed using the iterative method RAMLA LOR-3D, with a 144 × 144 matrix and pixel size of 4 × 4 × 4 mm^3. In particular, this dynamic acquisition provided 11 frames of 5 min each, leading to 11 data points of the experimental ^{18}F-FDG IF and of the experimental cancer tissue TAC, ranging 7.5–57.5 min post-injection. For determining the experimental ^{18}F-FDG IF, in each patient, a volume of interest (VOI) was drawn over the descending thoracic aorta in each frame of the dynamic acquisition yielding an intermediate ^{18}F-FDG blood TAC (i.e., intermediate IF). Then, the final IF was obtained through a calibration of the intermediate IF with the ^{18}F-FDG plasma value measured in a venous blood sampling performed at 45 min post-injection, that is, when an equilibrium is reached between ^{18}F-FDG concentration in arterial and vein blood [3, 16]. VOIs for IF and tissue TAC were semi-automatically placed over three

consecutive slices to include the five hottest voxels within the VOI.

Implementing Patlak's analysis, 3P-KMA, and 5P-KMA

Assuming that there may be a slow loss of the trapped tracer to the blood and when the analysis remains limited to data collected for the period $t > t^*$ after injection, that is, when the reversible compartments are in effective steady state with the blood plasma, Patlak and Blasberg derived a non-linear equation including a release rate constant (k_b) [8]:

$$A_T(t)/A_p(t) = \left[Ki \int_o^t A_p(\tau) e^{-K_b(t-\tau)} d\tau\right] / \left[A_p(t)\right] + V_b \quad (1)$$

$A_T(t)$ (in kBq mL^{-1}) is defined as the total tracer activity at time t per tissue volume unit that includes both trapped tracer and free tracer in the blood and interstitial volumes. $A_p(t)$ (in kBq mL^{-1}) is the blood activity at time t per blood volume unit, that is, the ^{18}F-FDG IF.

In each patient, Patlak's graphical analysis was implemented from Eq. 1, setting $k_b = 0$. Eleven cancer tissue TAC data points and the corresponding 11 data points of the experimental ^{18}F-FDG IF, ranging 7.5–57.5 min post-injection, were used. The lower limit of 7.5 min for this range was chosen in order to limit the analysis to data collected for the period $t > t^*$ after injection, as required by Eq. 1 validity [7, 8]. Ki was determined as the slope of the linear fitting of the Patlak's plot showing $A_T(t)/A_p(t)$ versus the ratio of time integral of the right hand side of Eq. 1 to $A_p(t)$, i.e., the so-called stretched time.

In each patient, 3P-KMA was implemented by first fitting the 11 data points of the experimental ^{18}F-FDG IF with a three exponentially decreasing function derived from Hunter's results, after data were uncorrected for the ^{18}F physical decay. Hunter's results were used, and not Vriens' ones as in previous studies, because the former were established with blood sampling performed at 55 min post-injection, in comparison with 25 min for the latter [12, 15–17]:

$$A_p(t) = A_0 \times [8.20 \times \exp(-9.3363 \times t) + 1.17 \times \exp(-\alpha_2 \times t) + \exp(-\alpha_3 \times t)] \quad (2)$$

In Eq. 2, the amplitude ratios of the three exponential functions and the time constant of the first exponential function (uncorrected for physical decay) were available from Hunter's results [16]. In each patient, A_0 (leading to virtual initial IF amplitude), α_2, and α_3 (time constants of the second and third exponential functions, uncorrected for physical decay) were obtained by fitting the experimental ^{18}F-FDG IF data points (XLSTAT Microsoft; Levenberg-Marquardt algorithm). Then, in each patient, a formula was established by analytically solving integral of Eq. 1 and by using the fitted three-exponential IF of Eq. 2 involving k_b [12, 15]:

$$\begin{aligned} A_T(t) = Ki \times A_0 \times \{&8.20 \times [\exp(-9.3363 \times t) - \exp(-(\lambda + k_b) \times t)]/[(\lambda + k_b) - 9.3363] \\ &+ 1.17 \times [\exp(-a_2 \times t) - \exp(-(\lambda + k_b) \times t)]/[(\lambda + k_b) - a_2] \\ &+ [\exp(-a_3 \times t) - \exp(-(\lambda + k_b) \times t)]/[(\lambda + k_b) - a_3]\} \\ &+ V_b \times A_p(t) \end{aligned} \quad (3)$$

In Eq. 3, the ^{18}F physical decay constant is λ, and Ki, k_b, and F were obtained in each patient by fitting the ^{18}F-FDG tissue TAC (XLSTAT, Microsoft; Levenberg-Marquardt algorithm), ranging 7.5–57.5 min post-injection, uncorrected for ^{18}F physical decay. Note that previous studies used ^{18}F-FDG tissue data obtained at late dynamic PET imaging, i.e., beyond 2 h after injection, in comparison with the current ones obtained at early imaging (7.5–57.5 min post-injection) [12, 15]. However, the rationale for deriving Eq. 3 remains identical, whatever the time of acquisition (>t* after injection).

In each patient, the 5P-KMA model was implemented on PMOD software by using the whole experimental IF and tissue TAC data points acquired from injection, with very short frames including the bolus injection (version 3.0; PMOD Technologies, Switzerland) [13]. The 5P-KMA model can provide four kinetic rate constants, i.e., K_1, $k_{2\text{-}3\text{-}4}$ and V_b: K_1 and k_2 account for forward and reversed transport between blood and reversible compartment, and k_3 and k_4 account for forward and reversed transport between reversible and trapped compartment, respectively [12, 15]. The rate constants Ki and k_b may be computed from K_1, $k_{2\text{-}3\text{-}4}$, as:

$$Ki = K_1 \, k_3/(k_2 + k_3) \quad (4)$$

$$k_b = k_2 \, k_4/(k_2 + k_3) \quad (5)$$

Statistical analysis

A normal distribution of the α_2 and α_3 values (Eq. 2) in the current study and in Hunter's study could not be clearly showed for each IF time constants; therefore, comparisons between the two studies were made by means of non-parametric Mann-Whitney's test (GraphPad Prism 6 software; two-tailed; 95% confidence level). Bland-Altman analysis was used for Ki comparison between 3P-KMA and Patlak's analysis, as well as for further comparisons between 3P-KMA and 5P-KMA, and between 5P-KMA and Patlak's analysis (GraphPad Prism 6 software; 95% confidence level) [18].

Results

Figure 1 shows an IF fitting in a typical patient. Values of A_0, α_2, and α_3 are presented for each patient in Table 1. Range of IF fitting correlation coefficients over the patient series was 0.989–0.999 (mean 0.996). The α_2 and α_3 values found in the current study were significantly lower than those of Hunter's study (after removing the decay correction): $P < 0.0001$ for the two comparisons.

Figures 2 and 3 show linear Patlak's fitting and non-linear 3P-KMA in the same patient as in Fig. 1. Values of Ki obtained from Patlak's analysis versus Ki, k_b, and V_b obtained from 3P-KMA are presented for each patient in Table 1. The range of correlation coefficients for Patlak's and 3P-KMA fitting over the patient series was 0.971–0.999 and 0.766–0.998 (mean 0.990 and 0.958), respectively. A significant correlation was found between correlation coefficients of IF fittings and those of 3P-KMA fittings ($R = 0.631$; $P < 0.01$; graph not shown).

3P-KMA Ki was found to be strongly correlated with Patlak's Ki ($R = 0.995$; $P < 0.001$; graph not shown). Figure 4 shows the comparison between 3P-KMA Ki and Patlak's Ki in the manner of Bland-Altman [18]. 3P-KMA Ki was significantly greater than Patlak's analysis Ki: Ki ratio (i.e., 3P-KMA/Patlak) which was 1.060 ± 0.040 on average (95% confidence limits), with 95% limits of agreement of 0.171. When patients with $k_b > 0$ were excluded ($n = 8$; Table 1), 3P-KMA Ki was no more significantly greater than Patlak's Ki: Ki ratio which was 1.014 ± 0.030 on average (95% confidence limits), with 95% limits of agreement of 0.098. A strong correlation was found between Ki ratio and k_b (Fig. 5; $R = 0.801$; $P < 0.001$).

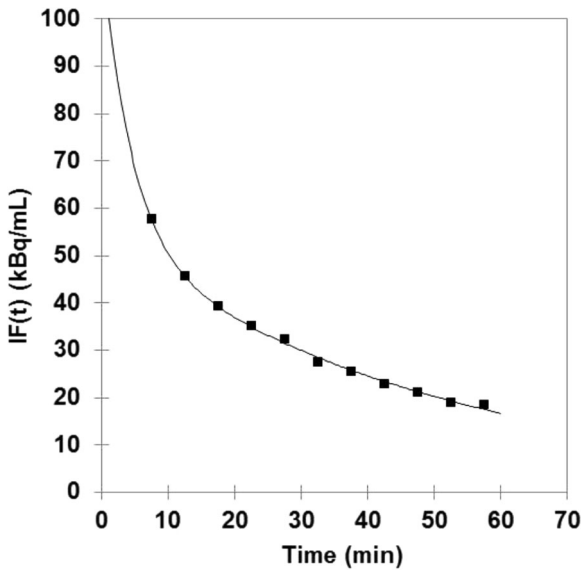

Fig. 1 Typical IF fitting (patient 9 in Table 1; $R = 0.989$; $P < 0.001$). PET data (square) are uncorrected for ^{18}F physical decay

Values of Ki, k_b, and V_b obtained from 3P-KMA and values of K_1, $k_{2\text{-}3\text{-}4}$, V_b, Ki, and k_b (computed from Eqs. 4 and 5) obtained from 5P-KMA are presented in Table 1. Range of correlation coefficients for 5P-KMA fitting over the patient series was 0.977–0.999 (mean: 0.989). 3P-KMA Ki was found to be strongly correlated with 5P-KMA Ki ($R = 0.989$; $P < 0.001$). No significant difference was found between 3P-KMA Ki and 5P-KMA Ki: Ki ratio (i.e., 3P-KMA/5P-KMA) which was 1.017 ± 0.054 on average (95% confidence limits), with 95% limits of agreement of 0.230. No significant difference was found between 5P-KMA Ki and Patlak's Ki: Ki ratio (Table 1) (i.e., 5P-KMA/Patlak) which was 1.056 ± 0.074 on average (95% confidence limits), with 95% limits of agreement of 0.317. 3P-KMA k_b was found to be significantly correlated with 5P-KMA k_b ($R = 0.60$; $P < 0.01$). No significant difference was found between 3P-KMA k_b and 5P-KMA k_b: k_b difference (i.e., 3P-KMA minus5P-KMA; k_b ratio is not allowed since division by zero is not allowed) which was 0.00041 ± 0.00083 min^{-1} on average (95% confidence limits), with 95% limits of agreement of 0.00359 min^{-1}. No significant correlation was found between 3P-KMA V_b and 5P-KMA V_b ($R = 0.12$).

Figure 6 shows the tissue TAC and the part of trapped tracer and of free tracer in blood and interstitial volume (Eq. 3), by using mean values for IF and for 3P-KMA parameters (Ki, k_b, V_b) obtained over the current lung cancer series.

Discussion

In each patient, 11 data points of the ^{18}F-FDG IF were fitted by using a three-exponential decreasing function. These data points ranged 7.5–57.5 min post-injection, that is, after an equilibrium has been reached between compartments in order to satisfy the Patlak's condition $t > t^*$. This function was derived from Hunter's results, of which A_0, α_2, and α_3 were obtained by fitting (Eq. 2) [16]. Indeed, the relative part of each exponential function to the IF area-under-curve (i.e., the total number of molecules that are available to the tissues after injection) is 1.14, 9.62, and 89.24% (by using the mean value of α_1 by Hunter and of α_2 and α_3 reported in Table 1), respectively. In other words, the part of the first exponential function in the whole IF, which mainly covers the IF peak, is very limited, suggesting that the mean value of α_1 reported by Hunter may be used in each individual [16]. Comparison between the fitted IFs of the current study and those reported by Hunter et al. shows that the former α_2 and α_3 values were significantly lower than the latter ones ($P < 0.0001$) [16]. The IF fitting correlation coefficients were high (range, 0.989–0.999; $P < 0.001$; Fig. 1). The major role of a reliable analytical IF as a sum of exponential functions for implementing 3P-KMA (Eq. 3) is emphasized by the significant correlation between IF fitting

Table 1 Fitting results in each patient for Patlak's analysis, 3P-KMA and 5P-KMA (A_0 in kBq mL^{-1}; α_2, α_3, k_b $k_{2\text{-}4}$ in min^{-1}; Ki and K_1 in mL min^{-1} mL^{-1}; V_b no unit)

Patient	A_0	α_2	α_3	Patlak's Ki	3P-KMA Ki	3P-KMA k_b	3P-KMA V_b	5P-KMA K_1	5P-KMA k_2	5P-KMA k_3	5P-KMA k_4	5P-KMA Ki	5P-KMA k_b	5P-KMA V_b
1	10.82	0.1210	0.0122	0.0329	0.0312	0.0000	0.08	0.0418	0.154	0.3615	0.0000	0.0293	0.0000	0.06
2	9.16	0.2283	0.0134	0.0308	0.0312	0.0000	0.07	0.0893	0.952	0.4250	0.0000	0.0276	0.0000	0.00
3	9.57	0.1442	0.0126	0.0806	0.0845	0.0008	0.20	0.1059	0.033	0.1401	0.0000	0.0859	0.0000	0.07
4	9.69	0.1470	0.0144	0.0376	0.0391	0.0000	0.22	0.1371	0.834	0.3091	0.0000	0.0371	0.0000	0.02
5	8.28	0.1069	0.0096	0.0192	0.0198	0.0000	0.18	0.0667	0.780	0.3351	0.0000	0.0201	0.0000	0.04
6	9.55	0.1288	0.0148	0.0366	0.0390	0.0000	0.13	0.1025	0.684	0.3083	0.0000	0.0319	0.0000	0.01
7	19.79	0.2130	0.0154	0.0471	0.0560	0.0012	0.16	0.1079	0.892	0.6850	0.0000	0.0469	0.0000	0.03
8	16.26	0.1580	0.0128	0.0368	0.0384	0.0000	0.07	0.0802	1.000	0.7798	0.0000	0.0351	0.0000	0.03
9	53.45	0.2245	0.0193	0.0403	0.0446	0.0018	0.03	0.1240	1.000	0.4740	0.0000	0.0399	0.0000	0.03
10	16.46	0.1527	0.0171	0.0352	0.0360	0.0000	0.25	0.1045	0.616	0.3115	0.0000	0.0351	0.0000	0.04
11	12.45	0.1347	0.0141	0.0363	0.0358	0.0000	0.12	0.1394	1.000	0.2935	0.0000	0.0316	0.0000	0.03
12	15.14	0.1579	0.0116	0.0157	0.0202	0.0056	0.28	0.0962	0.610	0.1871	0.0099	0.0226	0.0076	0.05
13	22.17	0.1345	0.0141	0.0222	0.0249	0.0026	0.33	0.1374	0.601	0.1434	0.0043	0.0265	0.0035	0.03
14	22.41	0.1137	0.0141	0.0124	0.0135	0.0000	0.28	0.1173	0.777	0.1269	0.0071	0.0165	0.0061	0.02
15	18.61	0.2594	0.0187	0.0165	0.0171	0.0000	0.23	0.0837	0.470	0.1501	0.0044	0.0202	0.0034	0.07
16	21.40	0.1317	0.0155	0.0384	0.0389	0.0000	0.07	0.0375	0.000	0.5850	0.9596	0.0375	0.0000	0.05
17	13.53	0.1472	0.0153	0.0297	0.0266	0.0000	0.04	0.0319	0.099	0.4346	0.0000	0.0260	0.0000	0.07
18	17.28	0.1964	0.0144	0.0273	0.0323	0.0046	0.09	0.1161	1.000	0.3852	0.0031	0.0323	0.0022	0.05
19	12.26	0.1636	0.0160	0.0305	0.0314	0.0011	0.25	0.1329	0.549	0.2267	0.0052	0.0388	0.0037	0.10
20	9.37	0.1075	0.0140	0.0647	0.0643	0.0000	0.22	0.1561	0.417	0.3546	0.0000	0.0717	0.0000	0.13
21	8.26	0.1353	0.0143	0.1310	0.1450	0.0002	0.10	0.1503	0.123	1.0000	0.0000	0.1338	0.0000	0.08
Mean	16.00	0.1574	0.0145	0.0391	0.0414	0.0009	0.16	0.1028	0.5995	0.3817	0.0473	0.0403	0.0013	0.05
SD	9.82	0.0426	0.0022	0.0263	0.0288	0.0016	0.09	0.0361	0.3454	0.2247	0.2091	0.0269	0.0023	0.03

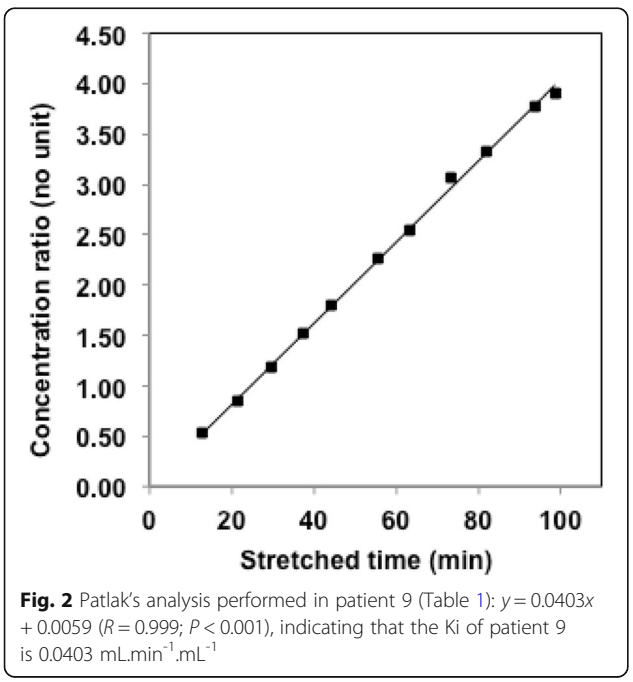

Fig. 2 Patlak's analysis performed in patient 9 (Table 1): $y = 0.0403x + 0.0059$ ($R = 0.999$; $P < 0.001$), indicating that the Ki of patient 9 is 0.0403 mL.min^{-1}.mL^{-1}

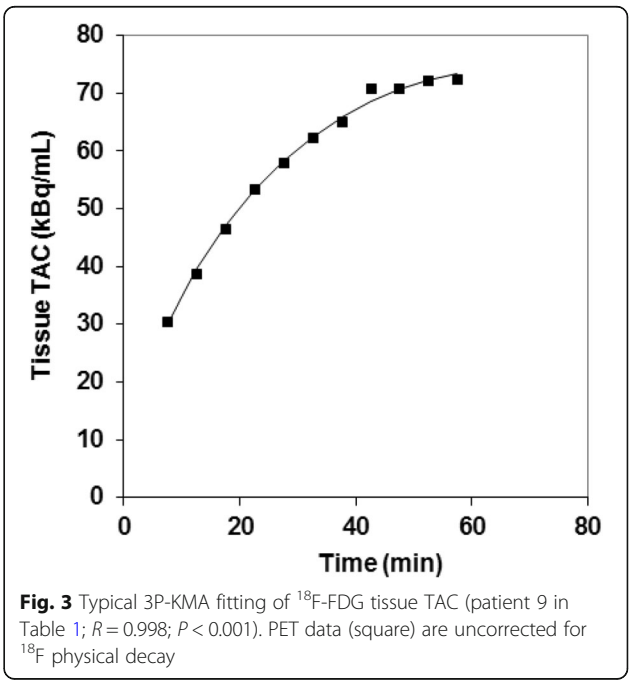

Fig. 3 Typical 3P-KMA fitting of ^{18}F-FDG tissue TAC (patient 9 in Table 1; $R = 0.998$; $P < 0.001$). PET data (square) are uncorrected for ^{18}F physical decay

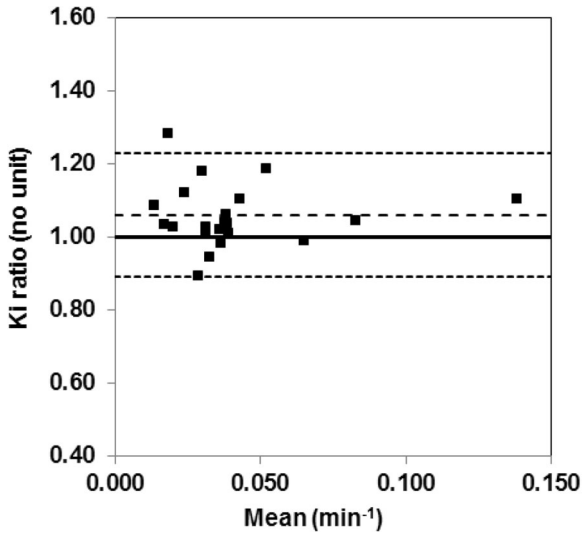

Fig. 4 Ki ratio of 3P-KMA/Patlak against mean. Ki ratio was 1.060 ± 0.040 on average (central dashed line; 95% confidence limits not shown), with 95% limits of agreement of 0.171 (upper and lower dashed lines)

correlation coefficients and those of 3P-KMA ($R = 0.631$; $P < 0.01$). It is noteworthy that, although the current study with ^{18}F-FDG used a three-exponential decreasing function, 3P-KMA may also be efficient with either a mono- or a bi-exponential IF depending on the tracer. Moreover, the ways the exponentially decaying IF can be obtained may be various: either from arterial or venous blood sampling, or image-derived, or from population-based IF models possibly scaled to later dynamic measurements on blood pool ROIs [3, 19].

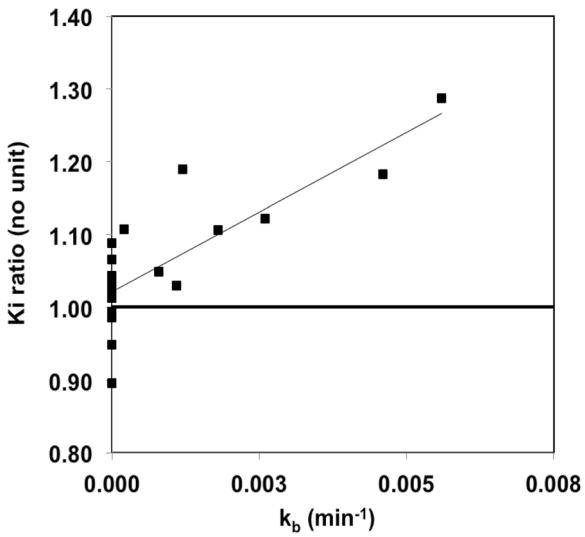

Fig. 5 Ki ratio of 3P-KMA/Patlak versus k_b: $y = 43.679x + 1.022$, $R = 0.801$; $P < 0.001$

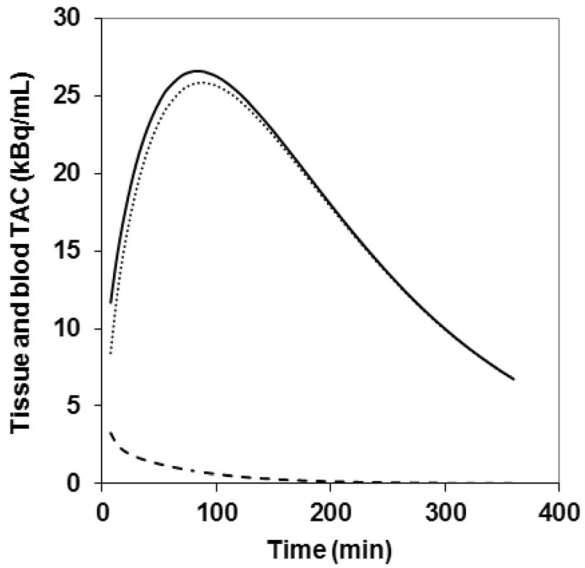

Fig. 6 (Full) Average tissue TAC obtained from mean values of the kinetic parameters (Ki, k_b, V_b) found over current lung cancer series; (dotted) trapped tracer TAC; (dashed) TAC of free tracer in blood and interstitial volume. Peak time for tissue TAC and trapped tracer TAC is 84 and 88 min, respectively. Data are uncorrected for ^{18}F physical decay

3P-KMA Ki was found to be 6.0% greater than Patlak's Ki, on average, with reasonable 95% limits of agreement of 17.1%, according to Bland-Altman analysis (Fig. 4). Moreover, when patients with $k_b > 0$ were excluded, 3P-KMA Ki was no more significantly greater than Patlak's Ki, with 95% limits of agreement of 9.8%. These findings were in agreement with Patlak and Blasberg's comment suggesting that, in case of reversible trapping ($k_b > 0$), linear fitting of a concave curve rather than that of a (true) linear one ($k_b = 0$), results in an underestimation of the slope and hence to Ki underestimation [8]. These findings also suggest that 3P-KMA and Patlak's analysis may be used interchangeably to assess ^{18}F-FDG uptake in lung cancer lesions. However, the strong correlation between Ki ratio (i.e., 3P-KMA/Patlak) and k_b (and hence, between Ki underestimation by Patlak's analysis and k_b; Fig. 5) suggests that 3P-KMA may be more appropriate than Patlak's analysis to accurately assess Ki in various ^{18}F-FDG-positive cancer lesions, possibly showing greater trapping reversibility than lung cancer lesions [9–11].

No significant difference over the current series was found between 3P-KMA Ki and 5P-KMA Ki and between 3P-KMA k_b and 5P-KMA k_b. A further comparison strengthens the current findings, between the current 3P-KMA outcomes and published ones by Dimitrakopoulou-Strauss et al., who implemented 5P-KMA in nine patients with lung tumors: Ki = 0.0414 ± 0.0288 min^{-1} (SD) and k_b = 0.0009 ± 0.0016 min^{-1} (SD)

for 3P-KMA (Table 1) versus the mean value of 0.0304 and 0.0009 min^{-1} for 5P-KMA by Dimitrakopoulou-Strauss et al., respectively [11]. However, it should be emphasized that the measurement uncertainty of the 3P-KMA outcomes may be expected to be lower than that of the 5P-KMA one because Ki and k_b from 5P-KMA has to be computed by using three independent kinetic (micro)parameters (Eqs. 4 and 5). As a result, the measurement uncertainty of Ki and k_b from 5P-KMA combines that of the three (micro)parameters, whereas the measurement uncertainty of Ki and k_b from 3P-KMA may be obtained without any further combination [20]. (Note that MU of 3P-KMA outcomes was not available from XLSTAT that did not allow a possible comparison with MU of 5P-KMA outcomes.) The proposed line of argument may be associated with Galli et al.'s results showing that close values of Ki may be computed from different set of (micro)parameter values [3]. It may also explain why, unlike for the comparison between 3P-KMA Ki and Patlak's Ki, no significant difference was found between 5P-KMA Ki and Patlak's Ki and, hence, that the Ki underestimation by Patlak's analysis was not revealed by the latter comparison. It may also be illustrated by the comparison of limits of agreement of 17.1 versus 31.7% that were found for the comparison between 3P-KMA and Patlak's analysis versus the comparison between 5P-KMA and Patlak's analysis, respectively. Furthermore, no significant correlation was found between 3P-KMA V_b and 5P-KMA V_b ($R = 0.12$), and the V_b mean value over the current series was found to be 0.16 ± 0.09 (SD) and 0.05 ± 0.03 (SD), respectively (Table 1). Consistently with the above-proposed comparison for Ki and k_b, comparison of the current 3P-KMA V_b value of 0.16 ± 0.09 (SD) with that of 0.17 ± 0.07 (SD) previously published for 5P-KMA by Dimitrakopoulou-Strauss et al. further strengthens the findings of the current study [11].

Unlike Patlak's analysis, the 3P-KMA approach allows expressing the whole tissue TAC as an analytical formula (Eq. 3). Therefore, at each time point, it is possible to compare it to that of its two components, that is, to the trapped tracer TAC and to the free tracer TAC. This comparison is shown in Fig. 6 by using mean values for IF and for 3P-KMA kinetic parameters that were obtained over the current lung cancer series (Table 1). Furthermore, this graph shows that the (mean) peak time for tissue TAC and trapped tracer TAC is 84 and 88 min, which could serve as landmarks to determine the optimal injection-acquisition time delay in clinical practice.

A limitation of the study is that, although the current 3P-KMA results obtained for Ki, k_b, and V_b were in agreement with previous literature results by Dimitrakopoulou-Strauss et al., the k_b/Ki ratio was low, about 2% on average in the current lung tumor series (Table 1) [11]. One could argue that 3P-KMA has been previously applied at late imaging to healthy liver that showed greater k_b values than those of lung tumors; however, we suggest that further studies are warranted to investigate the 3P-KMA efficiency in various tissues showing greater ^{18}F-FDG trapping reversibility than lung cancer lesions [9–11, 15]. Furthermore, we also suggest that future studies should compare the performance of the 3P-KMA non-linear fitting with that of a step-wise approach replotting non-linear graphical data with different values of k_b in order to recover a linear fitting and hence to obtain Ki [8]. Finally, the current study did not use respiratory gating and, in the case of lesions in the lower lobes, respiratory artifacts may very likely have affected outcomes of both 3P-KMA, Patlak's analysis, and 5P-KMA and thus might have had an influence on the reported SDs and limits of agreements.

Conclusions

Comparison between 3P-KMA and standard Patlak's analysis showed that the latter significantly underestimates, on average, the net influx constant (Ki) value in comparison with the former, because it arbitrarily set the release rate constant (k_b) to zero: the greater the k_b value, the greater the Ki underestimation. This underestimation was not revealed when comparing 5P-KMA and Patlak's analysis. We suggest that further studies are warranted to investigate 3P-KMA efficiency in various tissues, either physiological or pathological, showing greater ^{18}F-FDG trapping reversibility than lung cancer lesions.

Acknowledgements
Not applicable

Funding
The authors declare that they have no source of funding.

Availability of data and materials
Please contact author for data request.

Authors' contributions
EL conceived the 3P-KMA and participated in the study design and coordination and in the manuscript writing. MLC, GG, AG, AC, and LI carried out the PET scan acquisitions, obtained the IF and TAC data in all patients, implemented Patlak's analysis and 5P-KMA, and participated in the manuscript writing. RM participated in the study design, in the model interpretation, and in the manuscript writing. All authors read and approved the final manuscript.

Ethics approval and consent to participate
This is a retrospective analysis of a prospective study. All patients who were enrolled in the prospective study provided written informed consent before participating. The further retrospective study received the approval of the ethics committees of our teaching hospitals (Comité Régional Ethique Aquitaine and Comitato Etico, Università Cattolica del S. Cuore, Roma).

Consent for publication
Not applicable

Competing interests
The authors declare that they have no competing interests.

Publisher's Note

Author details
[1]Departments of Nuclear Medicine & Lung Function Testing, CHU de Bordeaux, Bordeaux, France. [2]Centre de Recherche Cardio-Thoracique, INSERM U-1045, Univ. Bordeaux, Bordeaux, France. [3]Physics Unit, Fondazione Policlinico Universitario "A. Gemelli", Roma, Italy. [4]Institute of Nuclear Medicine, Università Cattolica del Sacro Cuore, Roma, Italy. [5]Institute of Physics, Università Cattolica del Sacro Cuore, Roma, Italy. [6]Service de Médecine Nucléaire, Hôpital du Haut-Lévêque, Avenue de Magellan, 33604 Pessac, France.

Received: 25 January 2018 Accepted: 11 February 2018
Published online: 27 March 2018

References

1. Som P, Atkins HL, Bandoypadhyay D, et al. A fluorinated glucose analog, 2-fluoro-2-deoxy-D-glucose (F-18): nontoxic tracer for rapid tumor detection. J Nucl Med. 1980;21:670–5.
2. Huang HSC. Anatomy of SUV. Nucl Med Biol. 2000;27:643–6.
3. Galli G, Indovina L, Calcagni ML, Mansi L, Giordano A. The quantification with FDG as seen by a physician. Nucl Med Biol. 2013;40:720–30.
4. Laffon E, de Clermont H, Begueret H, Vernejoux J-M, Thumerel M, Marthan R, Ducassou D. Assessment of dual time point ^{18}F-FDG imaging for pulmonary lesions. Nucl Med Commun. 2009;30:455–61.
5. Sokoloff L, Reivich M, Kennedy C, et al. The |14C]deoxyglucose method for the measurement of local cerebral glucose utilization: theory, procedure, and normal values in the conscious and anesthetized albino rat J Neurochem 1977;28:897–916.
6. Phelps ME, Huang SC, Hoffman EJ, Selin C, Sokoloff L, Kuhl DE. Tomographic measurement of local cerebral glucose metabolic rate in humans with (F-18)2-Fluoro-2-deoxy-D-glucose: validation of method. Ann Neuro. 1979;6:371–88.
7. Patlak CS, Blasberg RG, Fenstermacher JD. Graphical evaluation of blood-to brain transfer constants from multiple-time uptake data. J Cereb Blood Flow Metab. 1983;3:1–7.
8. Patlak CS, Blasberg RG. Graphical evaluation of blood-to-brain transfer constants from multiple-time uptake data: generalizations. J Cereb Blood Flow Metab. 1985;5:584–90.
9. Okazumi S, Isono K, Enomoto K, et al. Evaluation of liver tumors using fluorine-18-fluorodeoxyglucose PET: characterization of tumor and assessment of effect of treatment. J Nucl Med. 1992;33:333–9.
10. Torizuka T, Tamaki N, Inokuma T, et al. In vivo assessment of glucose metabolism in hepatocellular carcinoma with FDG-PET. J Nucl Med. 1995;36:1811–7.
11. Dimitrakopoulou-Strauss A, Georgoulias V, Eisenhut M, et al. Quantitative assessment of SSTR2 expression in patients with non-small cell lung cancer using ^{68}Ga-DOTATOC PET and comparison with ^{18}F-FDG PET. Eur J Nucl Med Mol Imaging. 2006;33:823–30.
12. Laffon E, de Clermont H, Vernejoux JM, Jougon J, Marthan R. Feasibility of assessing [^{18}F]FDG lung metabolism with late dynamic PET imaging. Mol Imaging Biol. 2011;13:378–84.
13. Calcagni ML, Indovina L, Di Franco D, et al. Are the simplified methods to estimate Ki in ^{18}F-FDG PET studies feasible in clinical routine? Comparison between three simplified methods. Q J Nucl Med Mol Imaging. 2014;5 [Epub ahead of print]
14. Lammertsma AA. Forward to the past: the case for quantitative PET imaging. J Nucl Med. 2017;58:1019–24.
15. Laffon E, Adhoute X, de Clermont H, Marthan R. Is liver SUV stable over time in ^{18}F-FDG PET imaging? J Nucl Med Technol. 2011;39:1–6.
16. Hunter GJ, Hamberg LM, Alpert NM, Choi NC, Fischman AJ. Simplified measurement of deoxyglucose utilization rate. J Nucl Med. 1996;37:950–5.
17. Vriens D, de Geus-Oei L-F, Oyen WJG, Visser EP. A curve-fitting approach to estimate the arterial plasma input function for the assessment of glucose metabolic rate and response to treatment. J Nucl Med. 2009;50:1933–9.
18. Bland JM, Altman DG. Statistical methods for assessing agreement between two methods of clinical measurement. Lancet. 1986;1:307–10.
19. de Geus-Oei LF, Visser EP, Krabbe PF, et al. Comparison of image-derived and arterial input functions for estimating the rate of glucose metabolism in therapy-monitoring ^{18}F-FDG PET studies. J Nucl Med. 2006;47:945–9.
20. JCGM 100: 2008 . Evaluation of measurement data—guide to the expression of uncertainty in measurement; 2008. Available at: http://www.bipm.org. [Accessed September 2008].